Photoperiodic regulation of the seasonal pattern of photosynthetic capacity and the implications for carbon cycling

William L. Bauerle[a,b], Ram Oren[c,d,1], Danielle A. Way[c,e], Song S. Qian[c,2], Paul C. Stoy[f], Peter E. Thornton[g], Joseph D. Bowden[a], Forrest M. Hoffman[h], and Robert F. Reynolds[i]

[a]Department of Horticulture and Landscape Architecture, [b]Graduate Degree Program in Ecology, Colorado State University, Fort Collins, CO 80523; [c]Division of Environmental Science and Policy, Nicholas School of the Environment, Duke University, Durham, NC 27708; [d]Department of Forest Ecology and Management, Swedish University of Agricultural Sciences, SE-901 83, Umeå, Sweden; [e]Department of Biology, University of Western Ontario, London, ON, Canada N6A 5B7; [f]Department of Land Resources and Environmental Sciences, Montana State University, Bozeman, MT 59717; [g]Environmental Sciences Division/Climate Change Science Institute, [h]Computer Science and Mathematics Division, Oak Ridge National Laboratory, Oak Ridge, TN 37831; and [i]School of Agricultural, Forest, and Environmental Sciences, Clemson University, Clemson, SC 29634

Edited by Robert E. Dickinson, University of Texas at Austin, Austin, TX, and approved April 18, 2012 (received for review November 20, 2011)

Although temperature is an important driver of seasonal changes in photosynthetic physiology, photoperiod also regulates leaf activity. Climate change will extend growing seasons if temperature cues predominate, but photoperiod-controlled species will show limited responsiveness to warming. We show that photoperiod explains more seasonal variation in photosynthetic activity across 23 tree species than temperature. Although leaves remain green, photosynthetic capacity peaks just after summer solstice and declines with decreasing photoperiod, before air temperatures peak. In support of these findings, saplings grown at constant temperature but exposed to an extended photoperiod maintained high photosynthetic capacity, but photosynthetic activity declined in saplings experiencing a naturally shortening photoperiod; leaves remained equally green in both treatments. Incorporating a photoperiodic correction of photosynthetic physiology into a global-scale terrestrial carbon-cycle model significantly improves predictions of seasonal atmospheric CO_2 cycling, demonstrating the benefit of such a function in coupled climate system models. Accounting for photoperiod-induced seasonality in photosynthetic parameters reduces modeled global gross primary production 2.5% (~4 PgC y^{-1}), resulting in a >3% (~2 PgC y^{-1}) decrease of net primary production. Such a correction is also needed in models estimating current carbon uptake based on remotely sensed greenness. Photoperiod-associated declines in photosynthetic capacity could limit autumn carbon gain in forests, even if warming delays leaf senescence.

day length | gross primary productivity | carbon sequestration | leaf area index | evapotranspiration

Warming over the past 50 y has lengthened temperate growing seasons by 3.6 d per decade (1, 2). Longer growing seasons may increase net ecosystem productivity (2, 3), but increased spring carbon uptake has been accompanied by reduced autumn carbon uptake (2, 4). In extratropical ecosystems, where spring temperature is a major control on bud break, increased carbon sink strength has been linked to warmer April and May temperatures (3, 4), although drought can offset the increase in carbon uptake (5). The autumn switch from being a carbon sink to a carbon source in these ecosystems has been attributed to higher autumn temperatures, which are assumed to maintain high photosynthetic rates but even higher respiration rates (6). However, it is well known that leaf phenology responds to photoperiod, as well as temperature (7). Seasonal fluctuations in photosynthetic parameters are often modeled with temperature (8). However, photosynthetic physiology has also been shown to respond to photoperiod in controlled studies; instituting a short-day treatment in the fall, but maintaining high summer growth temperatures, inhibited the photosynthetic capacity of *Pinus banksiana* seedlings (9, 10). Seasonal measurements of photosynthetic capacity in trees under naturally changing photoperiod and air temperature signals are needed to ascertain whether maximum photosynthetic capacity declines when day length decreases.

Results and Discussion

We examined changes in leaf photosynthetic capacity (maximum carboxylation rates of Rubisco, V_{cmax}, and maximum electron transport rates, J_{max}) in 23 tree species, using both direct measurements of young, fully expanded leaves (11 species) and data on V_{cmax} from the literature (13 species, one overlapping with the previous set). In all cases, physiological function declined well before leaf shedding began (Fig. 1 *A* and *B*). We also measured changes in the leaf spectral index (LSI), a proxy for leaf compositional and spectral attributes [e.g., leaf nitrogen content, chlorophyll a + b concentration, absorption, reflectance, and greenness (11, 12)] (Fig. 1*C*). Although V_{cmax} and J_{max} began to decline in late June, there was no concurrent decrease in LSI. Leaf-shedding (gray bars in Fig. 1 *A*–*C*) began 5 wk after photosynthetic activity had ceased.

Because our measured trees received ample nutrients and water during the entire study period, the late season decline in photosynthetic capacity cannot be attributed to environmental stress, but may correlate with environmental signals. We used a nonlinear multilevel model (13) to determine when V_{cmax}, J_{max}, day length, and air temperature peaked, because the peak in physiological capacity should match or closely lag the dominant environmental signal. Because measurements cannot be made at the frequency required to capture the peak day of the year (DOY) of every species in every year, peaks for V_{cmax}, J_{max}, day length, and temperature were obtained by fitting a quadratic model for each separate species-year data (n = 4–28), an approach explicitly intended to estimate peak DOY for each parameter or variable (see *Methods* for further details). Across the V_{cmax} dataset, modeled photoperiod peaked on DOY 167 ± 1 (as opposed to the true peak on DOY 172), V_{cmax} peaked 3 d later on DOY 170 ± 6, and air temperature peaked a month later, on DOY 203 ± 1 (means ± between group SEs, lines in Fig. 1*A*). A similar pattern was seen for the J_{max} dataset, where photoperiod peaked on DOY 170 ± 1,

Author contributions: W.L.B., R.O., and P.E.T. designed research; W.L.B., J.D.B., and R.F.R. performed research; W.L.B., D.A.W., S.S.Q., P.C.S., P.E.T., and F.M.H. analyzed data; and W.L.B., R.O., D.A.W., S.S.Q., P.C.S., and P.E.T. wrote the paper.

The authors declare no conflict of interest.

This article is a PNAS Direct Submission.

[1]To whom correspondence should be addressed. E-mail: ramoren@duke.edu.

[2]Present address: Department of Environmental Sciences, University of Toledo, Toledo, OH 43606.

This article contains supporting information online at www.pnas.org/lookup/suppl/doi:10.1073/pnas.1119131109/-/DCSupplemental.

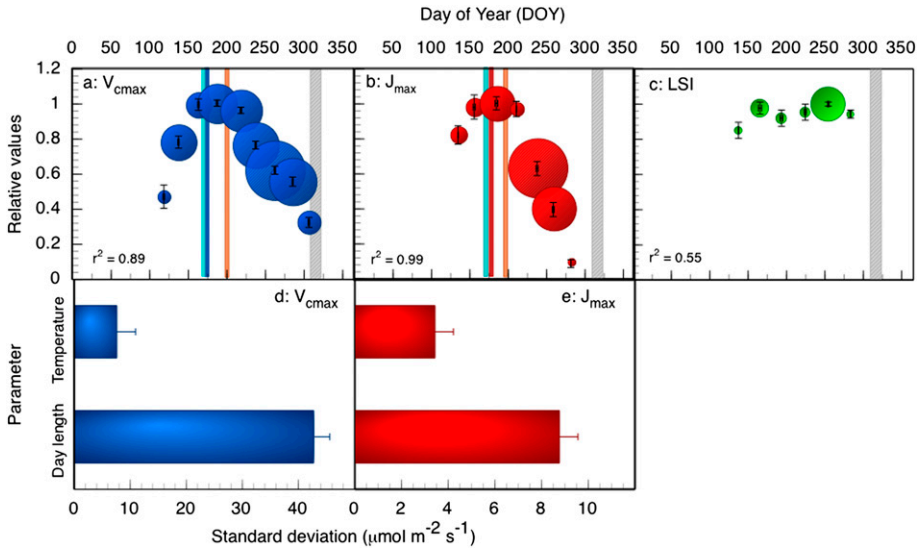

Fig. 1. Seasonal responses of photosynthetic physiology in 23 tree species. Binned averages (means ± SE) of measured changes in: (*A*) maximum Rubisco carboxylation rate (V_{cmax}), (*B*) maximum electron transport rate (J_{max}), and (*C*) leaf spectral index (LSI, a proxy for leaf nitrogen content, chlorophyll a + b concentration, and greenness characteristics) normalized by maximum calculated values for each species-year curve versus DOY and set at 1.0 for the maximum value of the bin means. Sample size in bins indicated by bubble diameter (n = 21–98 for V_{cmax}, 5–39 for J_{max} and 11–56 for LSI). Leaf shedding dates are indicated by the gray bars. Mean modeled peak DOY for day length (cyan lines), air temperature (orange lines), and (*A*) V_{cmax} (blue line) or (*B*) J_{max} (red line) from a mixed effect quadratic model, whose explicit purpose was to test relative locations of the peaks of photoperiod, temperature, and biological responses. SDs of variance components explaining seasonal variation in (*D*) V_{cmax} and (*E*) J_{max} (means ± SD). The SD shows how much variation is explained by each variance component when effects of the other variance components are already accounted for.

J_{max} peaked 9 d later on DOY 179 ± 4 and temperature peaked on DOY 194 ± 3 (lines in Fig. 1*B*). In both cases, leaf physiology peaked immediately after day length, decreasing as photoperiod declined, despite increasing air temperatures. To determine whether photoperiod or mean daily temperature was the dominant factor explaining variation in photosynthetic parameters, we used a variance components analysis (13). The variance components indicate the amount of variance explained by one factor when the effects of all other factors are considered. For both V_{cmax} and J_{max}, seasonal variation was mostly explained by photoperiod (or differences between individual curves from varying species-year combinations) and temperature was a nonsignificant factor (based on ANOVA) (Figs. 1 *D* and *E*).

To better establish the effect of photoperiod on photosynthetic physiology, we grew *Acer rubrum*, 'Red Sunset' saplings (one of the species from Fig. 1) at 25 °C under either natural photoperiod or an extended constant photoperiod of 16 h. Because there were few measurements before the summer solstice, we focus on the data postsolstice (Fig. 2). In saplings exposed to natural photoperiod, V_{cmax} declined after the solstice, (Fig. 2*A*) ($P < 0.0001$); V_{cmax} in the extended photoperiod treatment showed a declining trend ($P = 0.09$), but remained higher than in the natural photoperiod trees (time by treatment interaction, $P = 0.0014$, general linear model). Values of LSI were steady after the solstice in both treatments (Fig. 2*B*) ($P > 0.49$) and there was no predictive relationship between V_{cmax} and LSI in either treatment (Fig. 2*B*, *Inset*) ($P > 0.29$). Maximum values of light-saturated photosynthesis (A_{max}) showed similar seasonal patterns and treatment effects as V_{cmax} (Fig. S1).

Many coupled vegetation-climate models estimate photosynthesis using well-known relationships between V_{cmax} and environmental factors, such as air temperature and leaf nitrogen (14–16). Inconsistencies between different stomatal conductance and carbon assimilation models might be resolved by reducing V_{cmax}, but a physiological justification for this has been lacking (17). If maximum photosynthetic capacity is associated with day length, incorporating photoperiod effects should improve model results. In previous studies, accounting for day length effects on V_{cmax} in the Community Land Model (CLM) improved simulated annual cycles of gross primary productivity (GPP) at mid-to-high latitudes

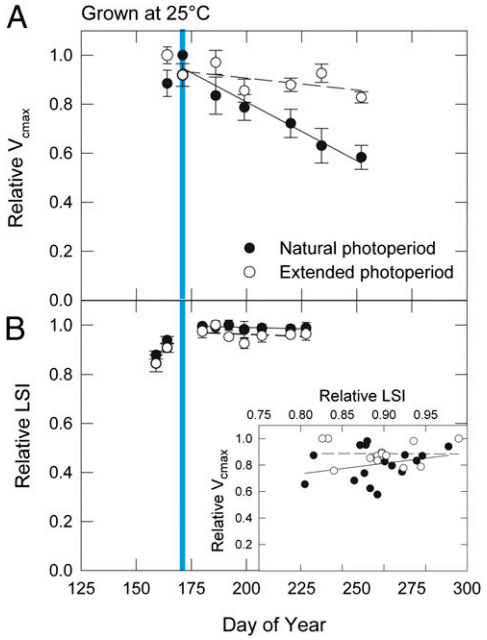

Fig. 2. Seasonal changes in (*A*) photosynthetic capacity (V_{cmax}) and (*B*) leaf spectral index (LSI) normalized by maximum measured values for each individual and set at 1.0 for the maximum value of the date means in saplings exposed to either naturally changing photoperiod (black circles, solid lines) or a constant extended photoperiod of 16-h (empty circles, dashed lines) (means ± SE, n = 2–4). Growth temperature was 25 °C in both treatments. Cyan bar indicates summer solstice. (*Inset*) Relationship between LSI and V_{cmax} from individual sapling data.

(18), and decreasing V_{cmax} allowed CLM to reproduce canopy level assimilation and transpiration observations (17). We therefore characterized the influence of a photoperiod correction of leaf physiology on global-scale terrestrial carbon cycling and carbon-climate feedbacks using CLM. We applied a simple multiplier to V_{cmax}, which scales from 1.0 on the summer solstice and follows the observed decline (Eq. **4**). Introducing a photoperiod correction reduced GPP, mainly in autumn at temperate and high latitudes in the northern hemisphere (Fig. 3). Global GPP decreased 2.5%, from 167.6 to 163.4 PgC y^{-1}, leading to a 3.4% reduction in global net primary production (NPP) from 58.7 to 56.7 PgC y^{-1}. The stronger influence on global-scale NPP relative to GPP is because of the concentration of the day-length effect in mid-to-high latitudes, where the modeled ratio of NPP:GPP is higher than the modeled global mean. Global mean leaf area index (LAI) was decreased by 3.0% which, combined with lower photosynthesis and stomatal conductance in the spring and autumn, drives a modeled reduction in global canopy transpiration of 2.5%. Lower LAI drives a 0.4% reduction in canopy evaporation of intercepted water. These changes together cause a 1.4% increase in ground evaporation and a 3.0% increase in runoff.

As an evaluation of introducing a day-length correction on a broadly integrative global-scale metric, we gauged model performance with and without a simple photoperiod control for 1988–2004 to assess the amplitude and phase of seasonal cycles of atmospheric CO_2 concentration, using the C-LAMP protocol and metrics (19), adding observations from the southern hemisphere. Although an earlier version of CLM-CN had an attenuated seasonal cycle of atmospheric CO_2 across the northern hemisphere (19), introduction of a photoperiod correction on V_{cmax} reduced bias and mean absolute error for seasonal cycle amplitude by 49% and 34%, respectively (mean of 60 stations globally) (Fig. 4 and Table S1). Improvements in seasonal cycle amplitude were observed in all latitude bands (Table S1), a result of sharpening the seasonal photosynthetic cycle in temperate regions by reducing autumn carbon uptake. Importantly, although the southern hemisphere maximum drawdown simulated without photoperiod control was delayed 2–3 mo compared with observations, photoperiod controls reduced this phase bias by approximately 1 mo (Fig. 4 and Table S1). This finding highlights that the improvements to the model are not just in the scale of carbon fluxes, but also in the seasonal timing of these fluxes. The small fractional changes in global total GPP translate to a large influence on seasonal cycle metrics as the seasonal cycle is driven by a small difference between several large opposing fluxes. Our modeling framework allows us to make a clean evaluation of adding the day-length correction mechanism, despite large observational uncertainty in the magnitude of the gross fluxes (20, 21).

In addition to improving the targeted process, the introduction of a new mechanism in a global model should not degrade performance in other parts of the model. Introduction of day-length control on V_{cmax} has a neutral or positive impact on all major categories of C-LAMP metrics, with especially large positive impacts on observation-based metrics of net carbon exchange at mid-to-high latitude flux stations (Table 1).

Maintenance of late season LSI is similar to the autumn "greening" detected by remote-sensing (22, 23), but was not indicative of extended photosynthetic activity (Figs. 1 and 2*B*, *Inset*). A positive linear correlation exists between nitrogen content and photosynthesis in fully functional leaves (24), leading to the expectation of a similar relationship between LSI (as a proxy for greenness and nitrogen content) and physiological activity (25). Many studies estimate seasonal courses in V_{cmax} and J_{max} from leaf nitrogen content, assuming a direct relationship (26, 27). However, although there is usually a positive relationship between photosynthesis and leaf nitrogen, the slope of this relationship is seasonally variable and can decline late in the growing season (28, 29), consistent with our observation that LSI is stable but photosynthetic capacity declines. Our results indicate that remotely sensed metrics of canopy activity based on a nitrogen or greenness signal (25) are likely to overstate forest carbon sequestration capacity under seemingly favorable autumn conditions.

Although the advance of the growing season with increasing spring temperatures is a potential positive effect of climate change on net ecosystem productivity (4, but see ref. 5), photoperiodic effects on late season physiological activity have been largely overlooked (9). We demonstrate late season declines in photosynthetic capacity of tree species despite favorable growing conditions. Photoperiod does not change from year to year or with climate. Thus, our results suggest that extended autumn growing seasons because of warmer temperatures may delay senescence, but will not necessarily enhance photosynthesis and carbon sequestration (5, 6). Assessments of carbon sequestration under a changing climate should consider limitations set by leaf physiological activity rather than by canopy leaf longevity. The responses of V_{cmax} and J_{max} to day length are the mechanisms explaining the seasonal pattern of photosynthetic rates, and the consequences of this pattern are reflected in atmospheric CO_2 and carbon sequestration. Although we cannot determine how photoperiod regulates photosynthetic capacity from our data, our results and previous data

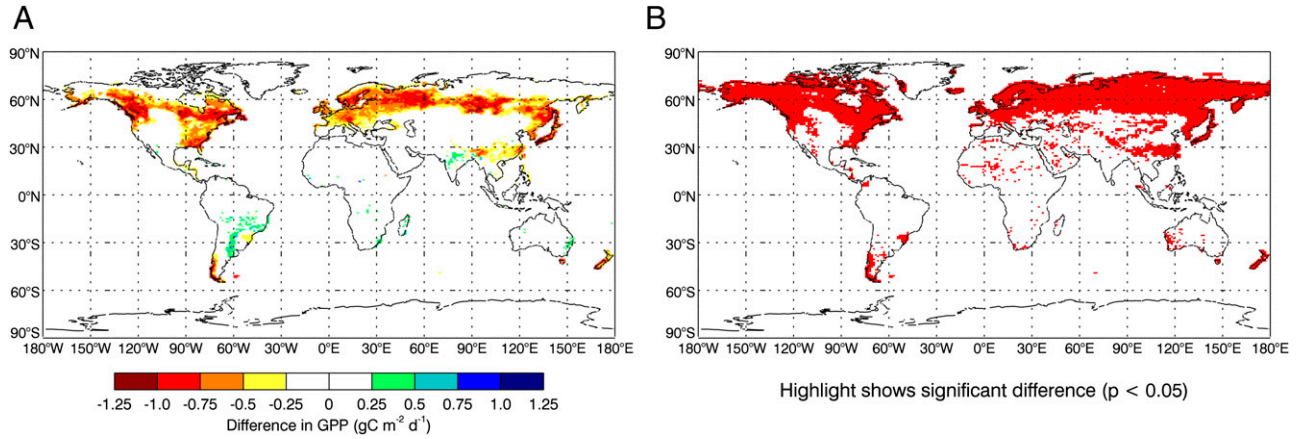

Fig. 3. Influence of a photoperiod correction of V_{cmax} on global distribution of GPP. (*A*) Difference in GPP (simulation with photoperiod correction minus simulation without) averaged over September, October, and November for the simulation period 1988–2004. (*B*) Red area indicates *P* value < 0.05 for two-tailed *t* test of significance for differences shown in *A*, where sample is based on 17 individual years.

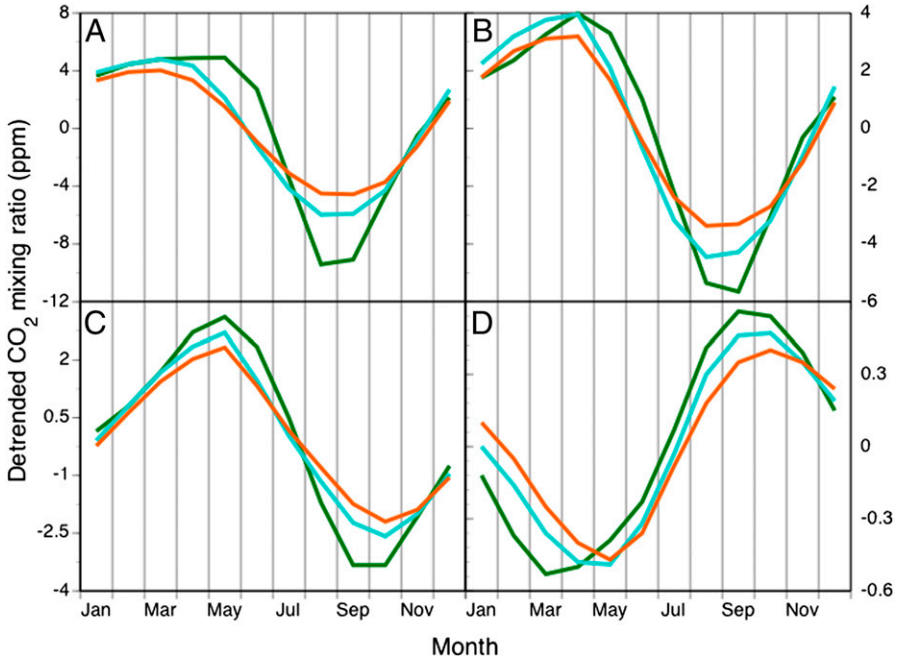

Fig. 4. Annual cycles of atmospheric CO_2 mixing ratio at (*A*) Alert, Nunavut, Canada (82.45°N), (*B*) Terceira Island, Azores, Portugal (38.8°N), (*C*) Mauna Loa, Hawaii, United States (19.5°N), and (*D*) South Pole, Antarctica. Observation-based estimates are from the GLOBALVIEW-CO2 product (43, 44) for years 1988–2004. Model estimates are detrended mean seasonal cycles from 1988 to 2004 from a simulation forced with reanalysis surface weather, historic CO_2 concentrations, historic nitrogen deposition, and historic land-use changes, and were obtained by impulse response function analysis (19). Results are shown for both the model without a day-length correction to V_{cmax} (orange line), and with a day-length correction to V_{cmax} (cyan line).

demonstrate that altering photoperiod (30) can directly alter leaf nitrogen and photosynthesis. Studies to ascertain the underlying mechanism by which photoperiod affects photosynthetic capacity, such as investigations of photoreceptor signal regulation, should be a priority for future research for incorporation into photosynthesis models. Unless ecosystem respiration acclimates to warmer temperatures (31, 32) or late season carbon fixation increases because of rising atmospheric CO_2 concentrations, warmer autumns could decrease annual carbon sequestration in forests (6). Models should incorporate day length as a correction function when predicting future warming effects on forest ecosystem productivity.

Methods

Leaf Physiology. We measured 11 field- and container-grown tree species (*Acer buergeranum* Miq., *Acer rubrum* L., *Betula nigra*, *Gleditsia triacanthos*, *Fraxinus pennsylvanica*, *Paulownia elongata*, *Paulownia fortunei*, *Prunus serrulata* Lindl. 'Kwanzan', *Prunus* × *yedoensis* Matsum., *Quercus nuttallii*, *Quercus phellos*) (33, 34) and one Freeman *Acer rubrum* cultivar (Autumn Blaze) over five growing seasons under nonresource limiting nursery conditions (34). Measured leaves were from continuously flushing, fully exposed, upper branches of 2.5- to 12-y-old saplings; leaf age was therefore similar across the growing season.

Biochemical photosynthetic limitations were measured using a portable steady-state gas exchange system (CIRAS-I and II; PP Systems). Leaves were acclimated to 25 °C air temperature, 1.3 kPa vapor pressure deficit, ambient atmospheric CO_2 concentrations (380–400 $\mu mol \cdot mol^{-1}$, depending on the sample and year) and a saturating photosynthetic photon flux density (PPFD; 1200 $\mu mol \cdot m^{-2} \cdot s^{-1}$) in the cuvettete until gas exchange was stable to determine initial net CO_2 assimilation rates (A_{net}, $\mu mol \cdot m^{-2} \cdot s^{-1}$). To determine V_{cmax}, cuvettete atmospheric CO_2 concentration (C_a) was sequentially lowered to 175, 150, 100, and 50 $\mu mol \cdot mol^{-1}$. C_a was then restabilized at 380–400 $\mu mol \cdot mol^{-1}$ to compare with initial A_{net} values to ensure open stomata and verify the stability of the measurements, after which C_a was increased to

Table 1. Summary of C-LAMP metrics for simulations with and without a photoperiod correction for V_{cmax}

Category	Possible score	Model without photoperiod correction	Model with photoperiod correction	Percent change because of introduction of photoperiod correction (%)
NPP	20	15.89	16.36	+3.0
LAI	15	11.50	11.74	+2.1
Carbon stocks	10	6.23	6.26	+0.5
Fluxnet*	20	11.56	11.75	+1.6
Fluxnet NEE†	5	1.98	2.22	+12.1
AmeriFlux‡	6	3.90	3.94	+1.0
AmeriFlux NEE§	1	0.41	0.46	+12.2
Fire variability	2	0.58	0.61	+5.2

Raw scores and percent changes are shown for major categories of C-LAMP metrics, and subscores are shown for net carbon fluxes at mid-to-high latitude stations (latitude > 45°N) in the Fluxnet and AmeriFlux categories. Positive changes indicate model improvements relative to observations. Details on observations and metrics are published elsewhere (19).

*Energy and carbon fluxes from Fluxnet.

†Net ecosystem exchange submetric for six stations with latitude > 45°N.

‡Energy and carbon fluxes from Ameriflux.

§Net ecosystem exchange submetric for 19 stations with latitude > 45°N.

600, 800, 1,000, and 1,200 μmol·mol^{-1} CO_2 to determine J_{max}. Photosynthetic light response curves were made on all species/genotypes before A_{net} – C_i curves were constructed; the light saturation point was never above 800 μmol·m^{-2}·s^{-1} in these measurements. To estimate biochemical limitations to carbon assimilation from A_{net} – C_i curves, the methodology of Wullschleger was followed (35). For each A_{net} – C_i curve, nonlinear regression explained >91% of the variation in A_{net} – C_i data.

The relative LSI seasonal change was estimated with a soil plant analysis development (SPAD) meter (model 502; Minolta Camera) (11, 12). We augmented our dataset with published seasonal measurements of V_{cmax} from 13 tree species (10 deciduous: *Acer rubrum* L., *Acer saccharum*, *Cercidiphyllum japonicum*, *Fagus crenata*, *Liriodendron tulipifera*, *Nyssa sylvatica*, *Platanus orientalis*, *Quercus alba*, *Quercus prinus*, and *Quercus serrata*; three evergreen: *Castanopsis cuspidata*, *Cinnamomum camphora*, and *Quercus glauca*) (29, 36–39). Data were digitized using Engauge Digitizer (version 4.1; http://digitizer.sourceforge.net/).

Extended Photoperiod Experiment. We grew 1-y-old *Acer rubrum* L. cv. Red Sunset under ample nutrient and water conditions in Colorado (latitude 40° 45′ N; longitude 105° 5′ W) in 26-L pots in a horticulture substrate (Fafard 52 mix, Fafard). Winter-dormant saplings were put in a controlled environment glasshouse until leaf out. In early summer, four replicates were randomly transferred to either a natural or extended photoperiod treatment in a glasshouse; temperature was 25 °C in both treatments. The extended photoperiod treatment maintained day length at 16 h; photoperiod varied in the natural treatment as day length changed (maximum light levels of 25.65 MJ·m^{-2} on DOY 172 in both treatments). Gas exchange was measured every 2 wk (see *Leaf Physiology* for methods); leaf age was similar across all measurements. Photosynthetic physiology was assessed as V_{cmax}; the relative LSI seasonal change was estimated with a SPAD meter (model 502; Minolta Camera). Five SPAD readings were recorded for each gas-exchange leaf.

Physiology Data Analysis. For the multispecies record, V_{cmax} and J_{max} data and their associated covariates (day length and daily mean temperature) from measurements of the same individuals of a single species in 1 y were grouped into one "curve" (V_{cmax}, 50 curves; J_{max}, 17 curves). Because the limited observations for each species-year curve (n = 4–28) made it unlikely that any measurement would capture the peak DOY, peak DOYs for V_{cmax}, J_{max}, day length, and temperature were obtained by fitting a quadratic model:

$$y = a(DOY - b)^2 + c + \varepsilon, \quad [1]$$

where b is the estimated peak DOY; r^2 for these curves used to estimate peaks from the multilevel analysis were 0.89 for V_{cmax} and 0.87 for J_{max}.

We used a nonlinear multilevel model for estimating the three coefficients in Eq. **1** by assuming that curve specific model coefficients a_j, b_j, and c_j share the same prior distribution:

$$\begin{pmatrix} a_j \\ b_j \\ c_j \end{pmatrix} \sim MVN\left(\begin{pmatrix} \mu_a \\ \mu_b \\ \mu_c \end{pmatrix}, \Sigma\right), \quad [2]$$

resulting in partial pooling of data from all curves. The emphasis of this model is on comparing the estimated b_j and its hyper-parameter μ_b for physiological measurements to the same temperature and day length.

Both photoperiod and air temperature were correlated with the photosynthetic parameters. Although V_{cmax} and J_{max} increase exponentially with a short-term (minutes to hours) linear increase in temperature (40), assuming a log-linear response of the physiological parameters to temperature also showed that photoperiod was the dominant factor in all cases; because the linear model was a simpler model and a better fit to the data (V_{cmax} – linear r^2 = 0.80, log-linear r^2 = 0.76; J_{max} – linear r^2 = 0.89, log-linear r^2 = 0.82), we present the linear model results. A variance components analysis was used to determine the dominant factor controlling variation in photosynthetic responses (13) by fitting a multiple linear model:

$$y_{ij} = \beta_{0j} + \beta_{1jdayl} + \beta_{2jtemp} + \varepsilon, \quad [3]$$

where j is the curve index, y is our physiological response variable, *dayl* is day length, and *temp* is air temperature. The Markov chain Monte Carlo simulation method was used to derive variance components (13).

For the extended photoperiod experiment, there was not a balanced design at every measurement, so we used a general linear model with time, replicate and treatment, nesting replicate within treatment.

Global Climate Model Simulation. We used the CLM (v4.0) (41), which includes coupled carbon and nitrogen cycle dynamics (14, 15). Simulations were performed on a global grid at ~1° × 1° resolution. The meteorological forcing data and spin-up procedure have been previously described (18). To test predicted carbon cycle dynamic sensitivity to late-season photoperiod regulation of photosynthetic potential, we used a day length-based scalar to modify photosynthetic potential:

$$V_{cmax,new} = V_{cmax,old}\left(\frac{dayl}{dayl_{max}}\right)^2, \quad [4]$$

where *dayl* and $dayl_{max}$ are the day length for a given day and the annual maximum day length, respectively. The form of Eq. **4** allows V_{cmax} to achieve its theoretical maximum on the summer solstice, with reductions in autumn corresponding to fractional declines in day length from its maximum value. The purpose of these simulations was to demonstrate the first-order effects of V_{cmax} photoperiod sensitivity on global carbon cycling and carbon-climate feedbacks. Given the improved model performance on multiple objective evaluation metrics, we suggest that a more refined implementation of this photoperiod logic be explored as a new model development activity.

The default parameterization of photosynthetic parameters in CLM-CN is based on leaf-scale measurements made during the peak growing season (15, 42). For simplicity, we applied a single day-length control for both deciduous and evergreen vegetation and across all latitudes in the global grid. Because the formulation of photosynthesis in CLM does not use J_{max}, relying instead on a constant parameterization of quantum efficiency for each vegetation type (41), we tested only the influence of day length on V_{cmax}.

ACKNOWLEDGMENTS. We thank Joe Landsberg, Elaine Poulin, and Dick Waring for comments on earlier drafts of the manuscript. This study was supported in part by the US Department of Agriculture, Horticulture Research Institute, Tree Research & Education Endowment Fund, South Carolina and Virginia Nursery and Landscape Associations, and Colorado and South Carolina Experiment Stations; US Department of Agriculture Grant 2009-51181-05768 and Cooperative Agreement 58-6618-2-0209 (to W.L.B.); the US Department of Energy, Office of Science, Biological and Environmental Research (R.O.); US Department of Agriculture Grant 2011-67003-30222; and the US Department of Energy, Office of Science, Biological and Environmental Research and the Natural Sciences and Engineering Research Council of Canada (D.A.W.). The Oak Ridge National Laboratory is managed by University of Tennessee–Battelle for the Department of Energy under Contract DE-AC05-00OR22725.

1. Menzel A (2003) Plant phenological anomalies in Germany and their relation to air temperature and NAO. *Clim Change* 57:243–263.
2. Keeling CD, Chin JFS, Whorf TP (1996) Increasing activity of northern vegetation inferred from atmospheric CO_2 measurements. *Nature* 382:146–149.
3. Goulden ML, Munger JW, Fan S-M, Daube BC, Wofsy SC (1996) Exchange of carbon dioxide by a deciduous forest: Response to interannual climate variability. *Science* 271:1576–1578.
4. Randerson JT, Field CB, Fung IY, Tans PP (1999) Increases in early season ecosystem uptake explain recent changes in the seasonal cycle of atmospheric CO_2 at high northern latitudes. *Geophys Res Lett* 26:2765–2768.
5. Angert A, et al. (2005) Drier summers cancel out the CO_2 uptake enhancement induced by warmer springs. *Proc Natl Acad Sci USA* 102:10823–10827.
6. Piao S, et al. (2008) Net carbon dioxide losses of northern ecosystems in response to autumn warming. *Nature* 451:49–52.
7. Körner C, Basler D (2010) Plant science. Phenology under global warming. *Science* 327:1461–1462.
8. Wang YP, Baldocchi D, Leuning R, Falge E, Vasala T (2006) Estimating parameters in a land-surface model by applying nonlinear inversion to eddy covariance flux measurements from eight FLUXNET sites. *Glob Change Biol* 13:652–670.
9. Busch F, Hüner NP, Ensminger I (2007) Increased air temperature during simulated autumn conditions does not increase photosynthetic carbon gain but affects the dissipation of excess energy in seedlings of the evergreen conifer Jack pine. *Plant Physiol* 143:1242–1251.
10. Busch F, Hüner NP, Ensminger I (2008) Increased air temperature during simulated autumn conditions impairs photosynthetic electron transport between photosystem II and photosystem I. *Plant Physiol* 147:402–414.
11. Peñuelas J, Filella I (1998) Visible and near-infrared reflectance techniques for diagnosing plant physiological status. *Trends Plant Sci* 3:151–156.
12. Richardson AD, Duigan SP, Berlyn GP (2002) An evaluation of noninvasive methods to estimate foliar chlorophyll content. *New Phytol* 153:185–194.
13. Gelman A, Hill J (2007) *Data Analysis Using Regression and Multilevel Hierarchical Models* (Cambridge Univ Press, New York).

14. Thornton PE, et al. (2009) Carbon-nitrogen interactions regulate climate-carbon cycle feedbacks: Results from an atmosphere-ocean general circulation model. *Biogeosci* 6: 2099–2120.
15. Thornton PE, Zimmermann NE (2007) An improved canopy integration scheme for a land surface model with prognostic canopy structure. *J Clim* 20:3902–3923.
16. Kucharik CJ, et al. (2000) Testing the performance of a dynamic global ecosystem model: Water balance, carbon balance, and vegetation structure. *Global Biogeochem Cycles* 14:795–825.
17. Chen HS, Dickinson RE, Dai YJ, Zhou LM (2011) Sensitivity of simulated terrestrial carbon assimilation and canopy transpiration to different stomatal conductance and carbon assimilation schemes. *Clim Dyn* 36:1037–1054.
18. Bonan GB, et al. (2011) Improving canopy processes in the Community Land Model version 4 (CLM4) using global flux fields empirically inferred from FLUXNET data. *J Geophys Res* 116:G02014.
19. Randerson JT, et al. (2009) Systematic assessment of terrestrial biogeochemistry in coupled climate-carbon models. *Glob Change Biol* 15:2462–2484.
20. Beer C, et al. (2010) Terrestrial gross carbon dioxide uptake: Global distribution and covariation with climate. *Science* 329:834–838.
21. Welp LR, et al. (2011) Interannual variability in the oxygen isotopes of atmospheric CO_2 driven by El Niño. *Nature* 477:579–582.
22. Myneni RB, Keeling CD, Tucker CJ, Asrar G, Nemani RR (1997) Increased plant growth in the northern high latitudes from 1981 to 1991. *Nature* 386:698–702.
23. Zhou LM, et al. (2001) Variations in northern vegetation activity inferred from satellite data of vegetation index during 1981 to 1999. *J Geophys Res* 106:20069–20083.
24. Reich PB, Walters MB, Ellsworth DS (1997) From tropics to tundra: Global convergence in plant functioning. *Proc Natl Acad Sci USA* 94:13730–13734.
25. Ollinger SV, et al. (2008) Canopy nitrogen, carbon assimilation, and albedo in temperate and boreal forests: Functional relations and potential climate feedbacks. *Proc Natl Acad Sci USA* 105:19336–19341.
26. Harley PC, Baldocchi DD (1995) Scaling carbon dioxide and water vapour exchange from leaf to canopy in a deciduous forest I. leaf model parameterization. *Plant Cell Environ* 18:1146–1156.
27. de Pury DGG, Farquhar GD (1997) Simple scaling of photosynthesis from leaves to canopies without the errors of big-leaf models. *Plant Cell Environ* 20:537–557.
28. Grassi G, Vicinelli E, Ponti F, Cantoni L, Magnani F (2005) Seasonal and interannual variability of photosynthetic capacity in relation to leaf nitrogen in a deciduous forest plantation in northern Italy. *Tree Physiol* 25:349–360.
29. Wilson KB, Baldocchi DD, Hanson PJ (2000) Spatial and seasonal variability of photosynthetic parameters and their relationship to leaf nitrogen in a deciduous forest. *Tree Physiol* 20:565–578.
30. Comstock J, Ehleringer JR (1986) Photoperiod and photosynthetic capacity in *Lotus scoparius*. *Plant Cell Environ* 9:609–612.
31. King AW, Gunderson CA, Post WM, Weston DJ, Wullschleger SD (2006) Atmosphere. Plant respiration in a warmer world. *Science* 312:536–537.
32. Luo Y (2007) Terrestrial carbon-cycle feedback to climate warming. *Annu Rev Ecol Evol Syst* 38:683–712.
33. Bowden JD, Bauerle WL (2008) Measuring and modeling the variation in species-specific transpiration in temperate deciduous hardwoods. *Tree Physiol* 28:1675–1683.
34. Reynolds RF, Bauerle WL, Wang Y (2009) Simulating carbon dioxide exchange rates of deciduous tree species: Evidence for a general pattern in biochemical changes and water stress response. *Ann Bot (Lond)* 104:775–784.
35. Wullschleger SD (1993) Biochemical limitations to carbon assimilation in C_3 plants-a retrospective analysis of the A/C_i curves from 109 species. *J Exp Bot* 44:907–920.
36. Kosugi Y, Matsuo N (2006) Seasonal fluctuations and temperature dependence of leaf gas exchange parameters of co-occurring evergreen and deciduous trees in a temperate broad-leaved forest. *Tree Physiol* 26:1173–1184.
37. Kosugi Y, Shibata S, Kobashi S (2003) Parameterization of the CO_2 and H_2O gas exchange of several temperate deciduous broad-leaved trees at the leaf scale considering seasonal changes. *Plant Cell Environ* 26:285–301.
38. Wilson KB, Baldocchi DD, Hanson PJ (2001) Leaf age affects the seasonal pattern of photosynthetic capacity and net ecosystem exchange of carbon in a deciduous forest. *Plant Cell Environ* 24:571–583.
39. Iio A, et al. (2008) Interannual variation in leaf photosynthetic capacity during summer in relation to nitrogen, leaf mass per area and climate within a *Fagus crenata* crown on Naeba Mountain, Japan. *Tree Physiol* 28:1421–1429.
40. Way DA, Sage RF (2008) Thermal acclimation of photosynthesis in black spruce [*Picea mariana* (Mill.) B.S.P.]. *Plant Cell Environ* 31:1250–1262.
41. Oleson KM, et al. (2010) Technical Description of version 4.0 of the Community Land Model (CLM). NCAR Technical Note. NCAR/TN-478+STR: 257.
42. White MA, Thornton PE, Running SW, Nemani RR (2000) Parameterization and sensitivity analysis of the Biome-BGC terrestrial ecosystem model: Net primary production controls. *Earth Interact* 4:1–85.
43. Masarie KA, Tans PP (1995) Extension and integration of atmospheric carbon dioxide data into a globally consistent measurement record. *J Geophys Res* 100:11593–11610.
44. GLOBALVIEW-CO2: Cooperative Atmospheric Data Integration Project - Carbon Dioxide. (2001) CD-ROM (National Oceanic and Atmospheric Administration Earth System Research Laboratory, Boulder, CO).